IEEE Access
Multidisciplinary ⋮ Rapid Review ⋮ Open Access Journal

Received May 31, 2018, accepted June 26, 2018, date of publication July 6, 2018, date of current version August 7, 2018.

Digital Object Identifier 10.1109/ACCESS.2018.2853666

Acoustic Emission for *In Situ* Monitoring of Solid Materials Pre-Weakening by Electric Discharge: A Machine Learning Approach

SERGEY A. SHEVCHIK[1], BASTIAN MEYLAN[1], ABBAS MOSADDEGHI[2], AND KILIAN WASMER[1], (Member, IEEE)

[1]Laboratory for Advanced Materials Processing, Swiss Federal Laboratories for Materials Science And Technology (Empa), 3602 Thun, Switzerland
[2]High Voltage Department, Selfrag AG, 3210 Kerzers, Switzerland

Corresponding author: Kilian Wasmer (kilian.wasmer@empa.ch)

This work was supported by the Swiss Commission for Technologies and Innovations (CTI), Non-destructive weakening analyses method for high voltage pulsed power technology, under Project CTI N°16024.1 PFEN-IW.

ABSTRACT Pre-weakening of solid materials using electric discharge is a new technique aiming at reducing significantly the costs and energy consumption as compared with the traditional raw materials processing in mining and recycling industries. However, the absence of an effective pre-weakening process monitoring and control prohibits its introduction into the market. The present contribution aims to fill this gap by investigating the feasibility of combining acoustic emission with machine learning for process monitoring. Hence, this paper is a supplement and enrichment of existing studies on *in situ* and real-time process monitoring and diagnosis associated with failure mechanism problems. Three categories and six subcategories are defined to describe the major pre-weakening scenarios of solid materials. The acoustic signals are collected and labeled according to the visual control of specially prepared transparent samples subjected to discharge exposure. The acoustic signals are decomposed with data adaptive M-band wavelets and the relative energies of the extracted frequency bands are used as features. Principal component analysis is applied to select the most informative features whereas several classifiers are applied to recognize the pre-weakening quality. The classification accuracy of the defined categories ranges between 84–93% demonstrating the applicability of the proposed method for *in situ* and real-time control of pre-weakening of solid materials using electric discharge.

INDEX TERMS Electric discharge, pre-weakening of solid materials, high voltage, underwater acoustic, M-band wavelet, support vector machine, machine learning.

I. INTRODUCTION

COMMINUTION (mechanical crushing and grinding of minerals) in mining and recycling industries is known to require a high energy consumption. Its share accounted for 0.4% of the total energy consumption of the USA in 2001 [1]. In mining countries, such as Canada, Australia or South Africa, this proportion raises up to 1 – 2% [1]. Therefore, any technology having the potential to reduce the energy consumption attracts attention. Today, pre-weakening of solid materials using high voltage electric discharge is the only solution that aims to induce multiple cracks inside a solid without necessary provoking its complete disintegration [2]–[4]. The preliminary trials by Cho *et al.* [4] and Bluhm [5] showed the potential of this technology for a significant reduction in energy consumption. Unfortunately, the lack of any *in situ* and real-time pre-weakening process monitoring and control systems prohibits this technology to be used in a wide practice. This is essentially due to the extremely complex physical phenomena taking place during the pre-weakening process. Actually, the only process control is made *ex situ* either via a drop weight test method [6] or JK Rotary Breakage Tester [7]. These methods require treating a large amount of samples and several steps of sieving and weighing to measure the size distribution of the broken pieces. The results are, then, compared with a reference sample (not treated by electric discharge) in terms of amount of energy requires to achieved a given particle size. Obviously, these manual methods are very time consuming (≈1 week per type of sample) and cost intensive. To face this issue, the development of process monitoring methodologies able

to check the process stability based on *in situ* and real-time sensing was indicated as a priority research area by many key mining companies. Hence, in this work, we propose to fill this gap with an innovative approach which combines acoustic emission (AE) with machine learning (ML) for *in situ* and real-time monitoring of pre-weakening of solid materials. The novelty of our method lies in mixing these three technologies, and in case of success, this will have a huge industrial potential.

Pre-weakening of solid materials with electric discharge exploits the dielectric properties of natural and most of construction materials (ores, natural rocks, cements, etc.). By adjusting the process parameters, the discharge can occur preferentially inside the material [4], [5], [8]. However, this process depends on the number and configuration of discharges induced cracks [7]. The pre-weakening quality is determined by comparing the amount of energy needed to mechanically fragment the solid materials with or without prior application of electric discharges [4], [5].

The high voltage pre-weakening process has been industrialized by SELFRAG AG [2], [9], [10] and their approach is to keep the process parameters, such as voltage and capacitance, within a certain dynamic range to guaranty that most of the material is pre-weakened. Though, the pre-weakening quality over the total processed volume is not constant. The reason is the complexity of the underlying physical phenomena [3], [11], [12] and strong heterogeneity and variability of both: the local dielectric and mechanical properties in the natural solid materials. Details on the physical phenomena of the discharge can be found in fundamental researches [3], [11], [12], while this study focuses on statistical analysis of the AE signals from the electrical discharge.

In the field of fracture mechanics, cracks initiation and propagation are investigated by means of acoustic emission (AE) as they induce stress waves [13]–[15]. The content of AE is an interference of acoustic waves from multiple local cracks and the AE intensity is proportional to the total number of all local crack events. Due to the stochastic nature of the pre-weakening process, the interpretation of AE remains a complex problem. Nevertheless, the feasibility of acoustic characterization of pre-weakening was shown for porous materials by Van Dalen [16]. Fourier signal analysis was applied to extract the AE frequency content and the unique combinations of frequencies for different pre-weakening scenarios were demonstrated. However, Fourier transform (FT) has known limitations when applied to non-stationary signals that are characterized by abrupt changes in frequencies [17]. Additionally, FT provides analysis only in the frequency domain, ignoring the development of the process in time. This prevents the identification of AE signals with identical Fourier spectra but with different pre-weakening consequences.

Analysis of AE in the time domain was reported by Grosse and Ohtsu [18] and Ohtsu [19]. The acoustic wave rise time, raise angle and oscillation around a fixed threshold were taken for describing the process on homogeneous materials in a well-controlled environment [15]–[19]. Unfortunately, this method cannot be employed for heterogeneous materials such as stones or ores in an industrial plant. The present study employed wavelets to analyze the pre-weakening AE signals. This choice was stipulated due to some advantages of this technique and the physical particularities of the discharge process in natural rocks. Wavelets provide the information in both, time and frequency domains and are free from the inherent constraints of the traditional Fourier transform while analyzing non-stationary signals [17]. The latter is important taking into consideration the non-stationary nature of the AE signals in the present application. At the same time, the discharge dynamics in natural rocks always follows several consecutive stages that alternate with one another [12]. This fixed scenario of the process development makes wavelets an optimal tool to capture the individual particularities of each stage in time domain. The further processing linked this valuable information with the pre-weakening impact within the machine learning framework described later. Wavelets were already successfully applied in a number of practical applications in the last decade and more details can be found in [20].

The products of wavelet decomposition are the narrow frequency sub-bands, localized in the time-frequency domain. In this contribution, the energies of those are used as features for the pre-weakening quality characterization. To reduce the approximation errors and to get a more detailed tiling of the time-frequency space, the data adaptive M-band wavelets were employed. The classification of the pre-weakening quality was carried out using three classifiers, namely: i) support vector machine (SVM), ii) random decision trees (RDT), and iii) feed-forward neural network (FFNN). Those represent three main state-of-the-art machine learning techniques that recommended as efficient analysis tools. At the same time, those methods are well developed, being a ready to use tool, thus minimizing the implementation time to industrialization.

The main objective of this work is to demonstrate the feasibility of combining AE and ML to monitor *in situ* and in real-time the pre-weakening taking place due to the discharge process. This is carried out by treating artificial transparent samples with similar properties to the rocks. The transparent samples ease the labelling directly of the acquired AE signals between the defined categories and subcategories. The collections of the AE signals are used to train and test the machine learning algorithm.

This paper has 4 sections. Section II presents the transparent artificial samples (TAS), the experimental setup for data acquisition and the particularities of the AE signals. Section III summarizes the extraction of the AE signal decomposition using M-band wavelets and computation of the energies of the narrow frequency bands, which are taken as features. The reduction of feature spaces using principal component analysis (PCA) is discussed and the classifiers are described. Section IV presents the categorization of pre-weakening quality in terms of industrial process significance and the classification results.

II. MATERIALS, EXPERIMENTAL SETUP AND ACOUSTIC DATA ACQUISITION

A. TRANSPARENT ARTIFICIAL SAMPLES (TAS)

The pre-weakening quality subjected to an electric discharge was studied by using specifically prepared transparent artificial samples; hereafter referred to as TAS. Those TAS allowed characterizing the discharge effects using post mortem visual inspection of the inner medium of the solids and to label the AE signals accordingly.

Two types of TAS were manufactured from two polymers based materials; poly methyl methacrylate (PMMA) were made from Clarofast powder from Struers GmbH (see Fig. 1a), and epoxy water-clear casting resin (epoxy resin) from R&G Faserverbundwerkstoffe GmbH (see Fig. 1b). The dielectric constants for PMMA and epoxy are 3 and 4, respectively, and so fit the range of dielectric constants of most natural solid materials (natural rocks) [21]. The dielectric properties of the TAS can be compared to the one of quartz, which is a component of a broad range of natural solid materials. In contrast, the dielectric strength of the PMMA and epoxy varies in the range of 15–20 MV/m and are higher as compared to the ones of natural solid materials (1.9 – 7 MV/m) [21]. Hence, to facilitate the dielectric breakdown of the TAS, a metallic pin was embedded inside the sample to provide an electric field enhancement, thus, increasing the probability to have the electric discharge inside the TAS medium. The pin is shown for the two types of TAS in Figs 1(a) and 1(b), and its position with respect to the electrodes is schematically shown in Fig. 1(c).

TAS with and without inclusions were produced. TAS with inclusions were used to simulate the disordered grain structure of real solid materials in a simplified way. The variations in the TAS inner structure provided a wider content in the AE signals. Several types of inclusions were incorporated into the TAS at various concentrations and different positions. As inclusions, glass pieces of various shapes (ball, cylinder, cube) and sizes (5–40 mm), were employed. Additionally, different inclusions made of various materials were employed as well and included table salt, mineral particles (2–8 mm) from magnetite (Fe_3O_4) and hematite (α-Fe_2O_3). Typical examples are presented in Fig. 1(a) and 1(b).

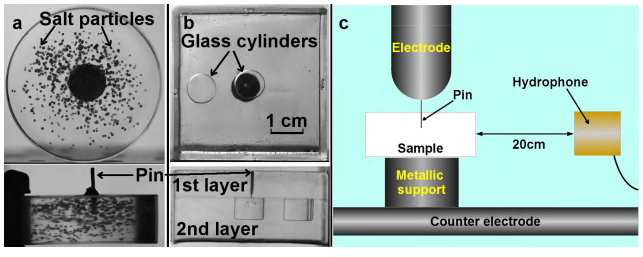

FIGURE 1. Transparent artificial samples (TAS) before electric discharge: (a) top and side views of a pressed PMMA sample with mineral inclusions and (b) a pressed epoxy sample with cylindrical glass inclusions, (c) schematic of the discharge chamber setup.

TAS made of PMMA without inclusions possessed a homogeneous medium and were manufactured by cutting off samples from a square rod of pure PMMA into slices with a thickness of 20 mm. In contrast, TAS made of PMMA with inclusions were produced by vacuum hot pressing of acrylic hot mounting resin powder (Clarofast from Struers GmbH) at 170°C and 25MPa for 15 min followed by cooling. The inclusions were incorporated inside the powder before hot pressing. These samples were produced as cylinders with a diameter and a thickness of 50 and 20 mm, respectively, and are shown in Fig. 1(a).

TAS from epoxy were produced by chemical reaction of the two components of the epoxy resin (Wasserklar from R&G Faserverbundwerkstoffe GmbH) inside a 50 mm square mold. To add inclusions, the epoxy samples were composed of two layers as shown in Fig. 1(b). After solidification of the first layer, the inclusions were placed inside the second layer at different positions.

B. HIGH VOLTAGE GENERATOR AND ACOUSTIC DETECTION

Discharge events inside the TAS were initiated using a big scale voltage generator from SELFRAG AG (Kerzers, Switzerland) [9]. It allowed tuning the operating voltage and storage capacitance in the range of 90–200 kV, negative polarity, and 2.5–37.5 nF, respectively. The voltage exposure of the TAS was carried out in a chamber filled with water. The setup was a standard industrial environment to provoke discharge preferentially inside the solid materials by applying short electric pulse (<50 μs). The setup is schematically represented in Fig. 1(c). The gap between the electrodes was set to 50 mm with the cathode (as the polarity is negative) touching the pin electrode of the TAS.

To produce a variety of damages in the TAS, several capacitance and voltage values were used. The corresponding AE signals were recorded simultaneously to the discharge via a record trigger. The detection of the acoustic signals was made directly inside the water filled chamber using an acoustic hydrophone sensor R30UC (Physical acoustics corporation, USA). It was grounded and placed at a distance of 20 cm from the electrode gap (Fig. 1(c)). The AE signals were recorded with a 10 MHz sampling rate and a duration of 16 ms. An electrical signal amplification of 20 dB was also applied.

It is important to mention the very high cost of a single experiment which is around 2-3 k€. This is a major limitation on the number of experiments that can be performed.

III. TIME-FREQUENCY ANALYSIS USING *M*-BAND WAVELETS

The uniqueness of our approach in this study is in the combination of AE sensors and the state-of-the-art machine learning (ML) method to monitor the pre-weakening of solid materials. This work is not the development of a new ML algorithm, but only the application of existing techniques and adaptation of those regarding the pre-weakening monitoring problem.

A. M-BAND WAVELETS

The analysis of the signals was carried out using M-band wavelet transform (MWT), which is a suitable technique for operating with non-stationary signals [22]. MWT is an extension of traditional wavelets [17] and is an alternative to the Fourier transform, expanding the analysis from only the frequency to the time-frequency domain. This is necessary since a discharge propagating inside a solid is a multistage process that evolves in time [12]. Therefore, wavelets are expected to capture the features of each process stage separately. The extension to MWT, as applied in this work, is made to operate at different signals subspaces, being sensitive to different process features. The MWT wavelet transform can be expressed as filtering the signal using M-channel quadrature filter bank [17]–[22]:

$$\varphi(n) = \sum_k h_0(k)\sqrt{M}\varphi(Mn-k), \quad k \subset Z \tag{1}$$

$$\psi(n) = \sum_k h_m(k)\sqrt{M}\varphi(Mn-k), \quad k \subset Z \tag{2}$$

where $m = 1, .., (M-1)$ is a channel number, h_o is a low pass filter and h_m are bands and high pass filters for $0 < m < M-1$, $m = M-1$, respectively, $\varphi()$ and $\psi()$ are the *approximation* and *details* coefficients, respectively, j is the current decomposition level, and n is the current sampling point of the digitized signal S. The wavelet function is characterized by the vanishing moments N, satisfying the condition: $\int n^k \psi(t)\, dt = 0$, where $k = 1, .., N$. The larger number of vanishing moments allows representing the complex signals with the smallest number of wavelet coefficients.

The full MWT includes multiple decomposition levels [17]–[22]. At each level, the split of the low frequency content (h_0) is carried out according to Eqs (1) and (2), resulting in the division of the signal into narrow frequency bands as illustrated in Fig. 2. Those narrow frequency bands are localized in time [17]–[22] and the ones from the band and high pass filters (h_m, $0 < m < M-1$) were taken for the further analysis following the scheme shown in Fig. 2(b).

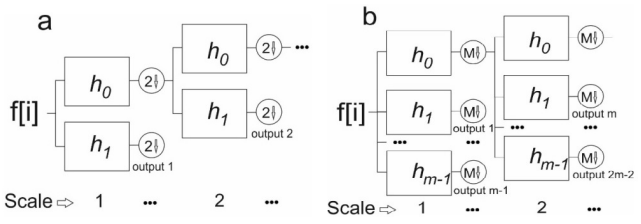

FIGURE 2. (a) Standard DWT, where h_0 and h_1 are the low pass and high pass filters respectively; (b) M-band DWT with M-channels, where h_0 is the low pass, h_1-h_{M-2} are narrow and h_{M-1} is the high pass filters.

The energy for each frequency band was computed according to:

$$E_{j,m} = \int \left|d_{j,m}(t)\right|^2 dt = \sum_k \left|d_{j,m}\right|^2 \tag{3}$$

where d are the wavelet or scale function coefficients extracted from Eqs (1) and (2). The relative energies were the normalized versions of the sub-band energies from Eq. (3), computed as:

$$\rho_{normj,m} = \frac{E_{j,m}}{E_j} \tag{4}$$

where $E_j = \sum_{k=0}^{M^j} \left|E_{j,m}\right|^2$ is the total energy accumulated in all frequency bands at a resolution level j. The results of Eq. (4) were considered as features and were the input of the classifier.

The choice of the wavelets is crucial to capture the local particularities of the signals [22]. For this reason, the data adaptive wavelets were used in this application. Several methods were considered for adaptive wavelets design [22]–[27]. We used the method proposed by Gupta *et al.* [22] as it had the best compromise between computational complexity and design limits. It also allows the construction of both, orthogonal and bi-orthogonal wavelet basis using the self-similarity as a global likelihood criterion. The other methods put some limitations in our specific application: a limited number of adaptive wavelets that is possible to design [23], [24], computational complexity in the case of many M-band channels [25], [26], the splines method is limited only to bi-orthogonal wavelets [27]. More details on the wavelet designed by Gupta *et al.* [22] are given in Section IV.C.

B. FEATURE SPACE REDUCTION

Before classification, the most informative features were preselected to avoid computational redundancy. We used principal component analysis (PCA) [28] to remove the non-informative features, thus, reducing the noise in classification input [28]. In other words, PCA allows saving computational time without losses in accuracy.

In PCA, the features from the original feature space U_0 are projected into a linear subspace U_1 with a lower dimension, which is a linear approximation of U_0. The projection is done following the expression [28]:

$$X_{U1} = w^T X_{U0} \tag{5}$$

where X_{U0} is the matrix of dimensions $[n, p]$ with the feature coordinates in the original space, X_{U1} are their projections, n and p are the numbers of measurements and the dimensionality of U_0, w is the principal components matrix with the weights $[w_1, \ldots, w_p]$. The projection w is chosen to provide with the maximum variance of Eq. (5):

$$max\{var\, X_{U1}\} = max\left\{var\, w^T X_{U0}\right\} = max\left\{w^T S w\right\} \tag{6}$$

where S is the covariance matrix of X_{U0} [28]. The solution of Eq. (6) can be obtained by a diagonalization of S using singular value decomposition. The elements in w are known as principal components and the selection of informative features is achieved by employing w with the greatest variance values. All details about PCA methods can be found in [28].

C. CLASSIFIERS

We tested three competitive machine learning techniques that are the state-of-the-art in classification tasks. First, support vector machine (SVM) was used as proposed by Cortes and Vapnik [29]. The technique analyses the features in the abstract feature space and tries to define the margin between the features from different categories. The margin search is an optimization problem that is solved during training with a labeled dataset [29], [30]. The advantage of SVM is in the possibility to process very complex features configurations in the feature space employing kernel trick [30]. In the present study, the radial based kernel (RBF) was used as it showed the best classification results [31].

Feedforward neural networks (FFNN) is another competitive technique with a high efficiency in classification tasks that is mainly due to the advances in the gradient propagation methods during its training. We employed a general implementation from da Silva *et al.* [32].

Random decision trees (RDT) is a probabilistic approach that constructs a number of tree classifiers, each of which splits the input data in individual way. The split rules are established during training and are based on features distributions within the training dataset. The final classification is a voting between many individual tree classifiers. The realization of the original algorithm from Breinman [33] was used, as it is state-of-the-art in classification efficiency [34].

IV. RESULTS AND DISCUSSIONS

A. ACOUSTIC EMISSION OF ELECTRIC DISCHARGE IN TAS

As already mentioned, natural solid materials possess a disordered grain structure, resulting in a stochastic development of discharge inside their medium. This causes a statistical diversity in the AE signals as illustrated in Fig. 3. Two TAS were subjected to electric discharges with identical voltage and capacitance of 160 kV and 20 nF, respectively. Both TAS were made of epoxy with glass inclusions of 5 mm diameter (Fig. 3(a1)) and 6–8 mm (Fig. 3(b1)). The inclusions had different configurations simulating a simplified model of the disorder in natural materials. They were placed at the periphery of the TAS in Fig. 3(a1) (TAS 1) and at its center in Fig. 3(a2) (TAS 2). The electric discharge resulted in the occurrence of multiple cracks without samples disintegration (pre-weakening). Under such circumstances, the stress wave propagation can be described as a cylindrically symmetrical process starting from the discharge area in the middle of the TAS and propagating to its periphery [12], [35]. This is confirmed when observing the cracks induced by the discharge in TAS 1 and TAS 2. The cracks propagate radially in different directions starting from the pin electrode in the middle of the TAS. The stochastic nature of cracks formation during the discharge is conditioned by the random distributions and configuration of inclusions, as well as the accumulated stresses inside the TAS. This is perfectly illustrated when comparing Fig. 3(a1) and 3(b1). The number and positions of the cracks formed are very different between both samples. Based on the inset of Fig. 3(a1), it can be seen that some inclusions were delaminated from the bulk materials. In contrast to TAS 1, some inclusions were damaged in TAS 2 as visible in the inset of Fig. 3(b1). This leads to a wide diversity of content in the emitted AE signals and evidence of this is in Fig. 3(a2) and 3(b2), where different distributions of the AE amplitude are observed. For example, a significant difference exists in the AE signals at 10 ms after the electric discharge onset. The TAS 2 is subjected to abrupt changes in frequency content. We believe that the non-stationary behavior of the AE, shown in the inset in Fig. 3(b2), is due to individual crack emission of acoustic waves. Besides, differences in the AE content are visible when comparing both signals between 2 and 7 ms after the process initiation (see Fig. 3(a2) and 3(b2)).

The frequency energy distribution for both samples is presented as sonograms in Fig. 3(a3) and 3(b3). The crack

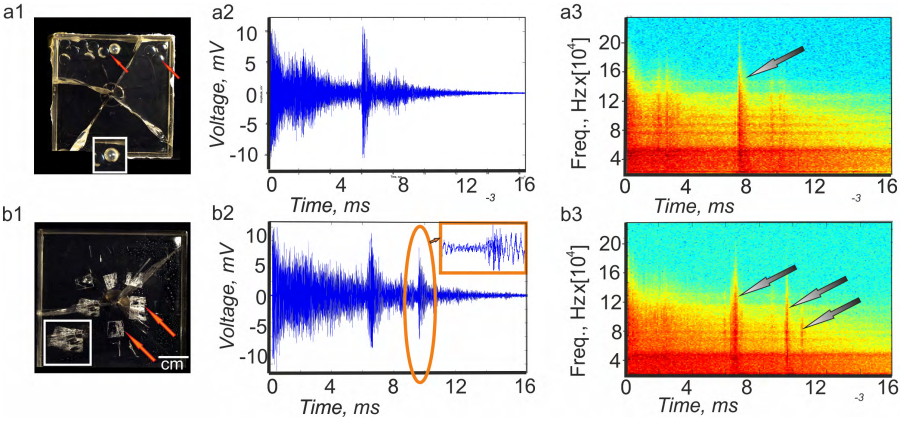

FIGURE 3. (a1) and (b1) are top views of TAS 1 and TAS 2, respectively, after an electric discharge. The red arrows mark the inclusions; (a2) and (b2) are AE signals of the electric discharge in TAS 1 and TAS 2, respectively; (a3) and (b3) are the sonograms of AE signals from TAS 1 and TAS 2, respectively. Both samples were exposed to the same electric discharge with voltage and capacitance of 160 kV and 20 nF, respectively.

formation frequencies fit the range 0–160 KHz, although the distribution of those within this range differs for each TAS. The differences in the AE released are indicated by the arrows in the sonograms in Fig. 3(a3) and 3(b3). Each signal includes a random number of fluxes that occurs at random time. The challenge in the classification of such signals is in the extraction of a fixed combination of frequencies that uniquely characterize each pre-weakening category.

B. SIGNALS CATEGORIZATION AND AE DATASET

The number of experiments was limited due to the high experimental cost. Thus, this investigation was carried out on 205 manufactured TAS, from which 86 were made using PMMA and the other 119 from epoxy (See Section II.A). All samples were exposed to electric discharges with voltage and capacitance in the range of 90–180 kV and 2.5–25 nF, respectively. Most samples were treated with multiple discharges until the desired pre-weakening state was reached. The AE signal from each electric discharge was recorded leading to a total dataset with 500 AE signals. Each TAS was visually controlled after each treatment. According to this, the AE signals were divided into several categories and subcategories. Table 1 presents the categorization and labeling of the collected AE signals. It contains three main categories and each is divided into two subcategories. The categories describe the electric discharge propagation, while the subcategories indicate the electric discharge efficiency in terms of pre-weakening. In Table 1, the number of collected AE signals and tested samples are given without/with brackets, respectively. Figure 4 shows representative optical microscope images with the corresponding AE raw signals of the main categories and subcategories.

TABLE 1. Categories, subcategories and labeling of the AE dataset results.

Nº	Categories	Training dataset		Test dataset	
	Subcategories	PMMA	Epoxy	PMMA	Epoxy
1	**Discharge in TAS**	**45 (35)**	**50 (47)**	**9 (9)**	**39 (39)**
1.1	Pre-weakening	33 (23)	32 (29)		24 (24)
1.2	Break-down	12 (12)	18 (18)	9 (9)	15 (15)
2	**Discharge fail**	**89 (24)**	**40 (14)**	**78 (16)**	**60 (11)**
2.1	No discharge	30 (5)		34 (7)	34 (7)
2.2	Discharge tree	59 (19)	40 (14)	44 (9)	26 (4)
3	**Surface discharge**	**34 (24)**	**62 (43)**	**62 (19)**	**54 (21)**
3.1	Without pre-weak.	12 (9)	24 (18)	44 (11)	27 (5)
3.2	With pre-weak.	22 (15)	38 (25)	18 (8)	27 (16)

Without brackets denotes the number of collected AE signals; in brackets, the number of tested samples

The category ***discharge in TAS*** is of utmost importance for the industries and contains the subcategories *pre-weakening* and *break-down*. The optical views and their respective AE signals are illustrated in Fig. 4(a) and 4(b). In both subcategories, the discharge area is visible at the center of the sample from which multiple cracks are propagating. Figure 4(a), *pre-weakening,* is a side view of a TAS made of PMMA after a discharge exposure of 120 kV and a capacitance of 8 nF.

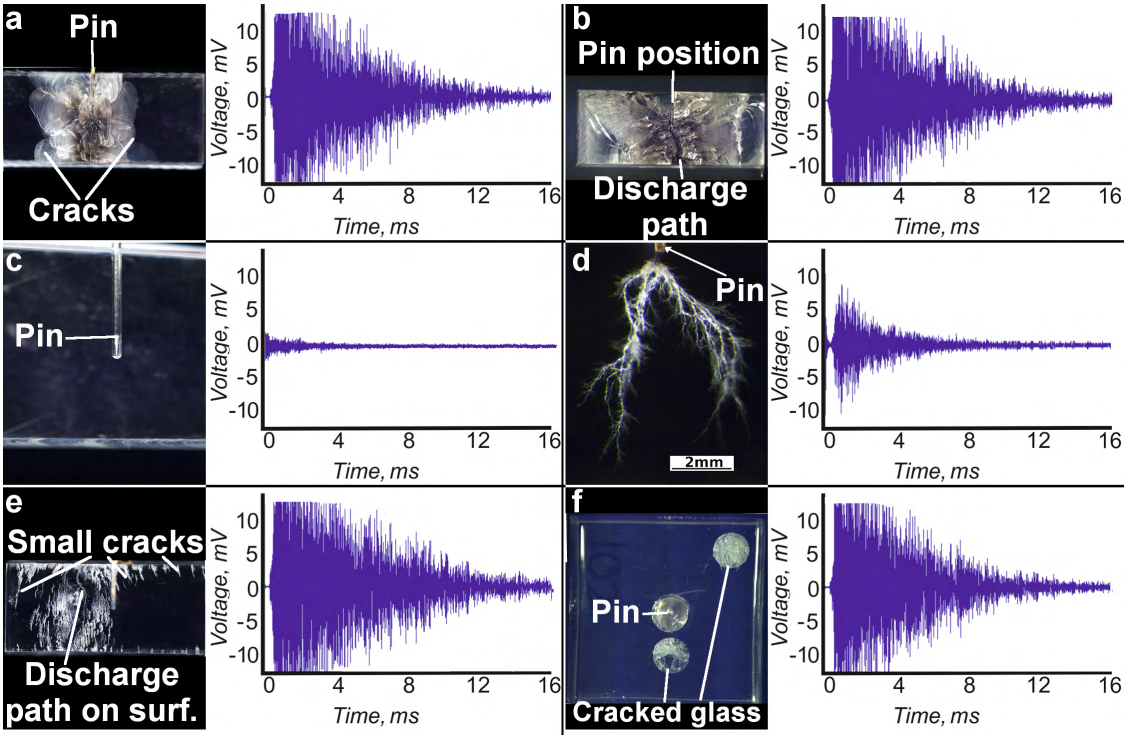

FIGURE 4. Representative optical microscope views of all categories and subcategories of the TAS subjected to an electric discharge and their respective AE recorded signals. The categories and the subcategories are respectively (a) discharge in TAS, pre-weakening; (b) discharge in TAS, break-down; (c) discharge fail, no discharge; (d) discharge fail, discharge tree; (e) surface discharge, without pre-weakening; (f) surface discharge, with pre-weakening.

Cracks are observable around the pin electrode zone and are confined within the sample without propagation to its edges, preventing its disintegration into pieces resulting to no material losses. The path of the electric discharge is also visible. In contrast, the TAS belongings to the subcategory *break-down*, Fig. 4(b), are easily recognized as the cracks are propagating to the edges leading to the breakage of the TAS in several separate parts. In this figure, the discharge path is observed on a fragment (approximately half of the sample) issue from the disintegration of the PMMA sample after a discharge exposure of 160 kV and a capacitance of 12.5 nF. The signals from both subcategories (*pre-weakening* and *break-down*) showed similarities and the signal attenuations reach a noise level at about 15 ms. For industries, the category ***discharge in TAS*** is the desired process as it weakened the solid materials at most with the least energy consumption.

The category ***discharge fail*** is defined when no or partial discharges occurred. It is divided into two subcategories *no discharge* and *discharge tree*. *No discharge* occurs when the voltage of the electric discharge is lower than the dielectric strength of the TAS. Hence, *no discharge* produces simply a so-called machine click but has no effect on the TAS as illustrated in Fig. 4(c). This figure is a side view of a PMMA sample after an unsuccessful discharge treatment at 160kV with a capacitance of 8.5 nF. The signals from this subcategory were used for estimating the intrinsic noise of the generator. The corresponding frequency sub-bands were removed from further analysis. For the experiments falling in this subcategory, the TAS were treated iteratively by increasing the voltage until the dielectric break-down level is exceeded and the electric discharge took place and produced some damages. In the opposite, a partial discharge creates already some small damages in the TAS in the form of *discharge tree*. This is illustrated in Fig. 4(d), with a side view of the pin electrode area of a TAS made of PMMA treated with an electric discharge of 120 kV and 2.5 nF. In this figure, a tree reflecting light is visible starting from the tip of the pin. The nature of this structure is hollow channels inside the TAS medium created by plasma formation. This is confirmed by visual observation during the discharge where a bright light is visible at the location of the tree. Such events takes place when the applied voltage was enough to start the dielectric break-down and provide the growth of the streamer towards the counter electrode, but the energy of the discharge was low and was absorbed by the TAS medium before reaching the counter electrode. For the two subcategories, *no discharge* and *discharge tree*, all TAS preserved their integrity and their AE signals are characterized by a low acoustic energy and short duration as seen in the AE signals in Fig. 4(c) and 4(d).

The category ***surface discharge*** corresponds to a discharge occurring in the surrounding water environment or at a surface of the TAS. This happens when the break-down voltage of the interface TAS/water is lower than the one of the TAS. The surface discharge has two consequences that are described by the subcategories *without pre-weakening* and *with pre-weakening* in Table 1. The subcategory ***surface discharge*** *without pre-weakening* is easily recognized by scratches on the TAS surface as shown in Fig. 4(e), which shows a side view of a TAS made of PMMA. Actually, in this specific case, no cracks inside the TAS medium are observed but only surface damage and traces indicating the discharge propagation path are visible. Noteworthy, despite having a discharge occurring outside the TAS, crack formations are still possible due to the propagation, through the sample, of pressure waves induced by the outer electric discharge. Such events are categorized in the next subcategory ***surface discharge*** *with pre-weakening*. To achieve this state, the energy of the pressure waves entering the sample has to be equal or higher than the energy required for cracks initiation. Therefore, this phenomenon is observed almost exclusively in TAS with brittle inclusions such as glass. This is represented in Fig. 4(f), which is a top view of a TAS made of epoxy treated with an electric discharge of 120 kV and 2.5 nF. The glass inclusions (glass cylinder of 8 mm diameter and 10 mm height) have many cracks induced by the surface discharge. The epoxy matrix is intact around the inclusion. The cracks occur mainly close to the TAS surface as most cracks are visible on the inclusion closest to the corner and gradually disappeared while propagating into the TAS center, where the inclusion close to the center is almost intact. This cracking behavior is in opposition with the one of discharge inside where the cracks propagate from the center of the TAS as shown in Figs 3(a), 3(b), 4(a) and 4(b).

Comparing all AE signals in Fig. 4, we perceive that the ones from ***discharge in TAS*** and the ***surface discharge*** have close identity in both time duration and amplitude levels. Taking into account the number of cracks caused by each individual electric discharge, the AE classification is challenging and the results of its applicability will be discussed in Section IV.E. For reducing the costs and energy consumption of raw materials processing in mining and recycling industries, the subcategories 1.1, 1.2 and 3.2 in Table 1 are crucial as they provide the desired solid materials treatment.

C. DATA ADAPTIVE WAVELET

The design of the data adaptive wavelet for the collected AE signals was carried out using a mix of the AE signals collected, chosen randomly from all categories, described above. The method from Gupta *et al.* [22] was applied for the wavelet design. The choice of the designed M-band wavelets vanishing moments and the total number of wavelets channels was made via an exhaustive search to minimize the approximation error. The best wavelet approximation was achieved having 4-band wavelet and 5 vanishing moments. The parameters of the designed wavelet are presented in Table 2, whereas Fig. 5 is the computed 4-band data adaptive wavelet. The application of the 4-band wavelet allowed to tile the time - frequency space into separate frequencies with bands that fit the range from approximately 9.7 kHz to 2.5 MHz. The

TABLE 2. High, narrow band and low pass filters for using the *M*-band wavelet.

h_0 = [0.03124, 0.05237, -0.00767, 0.00588, 0.96700, 0.00121, -0.00298, 0.01266, 0.03046, 0.048127]
h_1 = [0.02321, 0.04054, -0.00699, 0.00726, 1.00000, 0.00011, -0.01328, 0.01381, 0.01516, 0.036536]
h_2 = [0.02029, 0.03192, -0.00459, 0.00956, 1.00000, 0.00014, -0.01191, 0.01014, 0.00633, 0.034321]
h_3 = [0.01958, 0.03187, -0.00739, 0.00809, 1.00000, 0.00014, -0.01103, 0.01537, 0.00058, 0.026485]

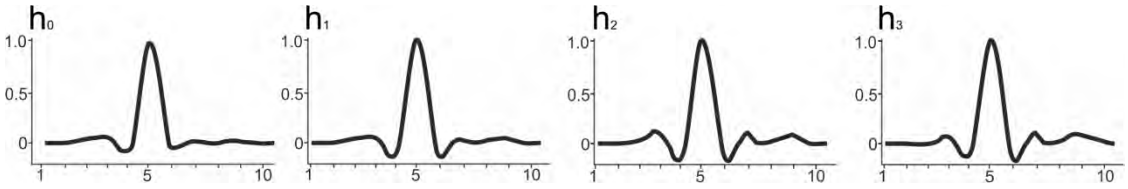

FIGURE 5. The 4-band data adaptive wavelet computed with the method described in Gupta *et al.* [22] using the signals collected from the TAS.

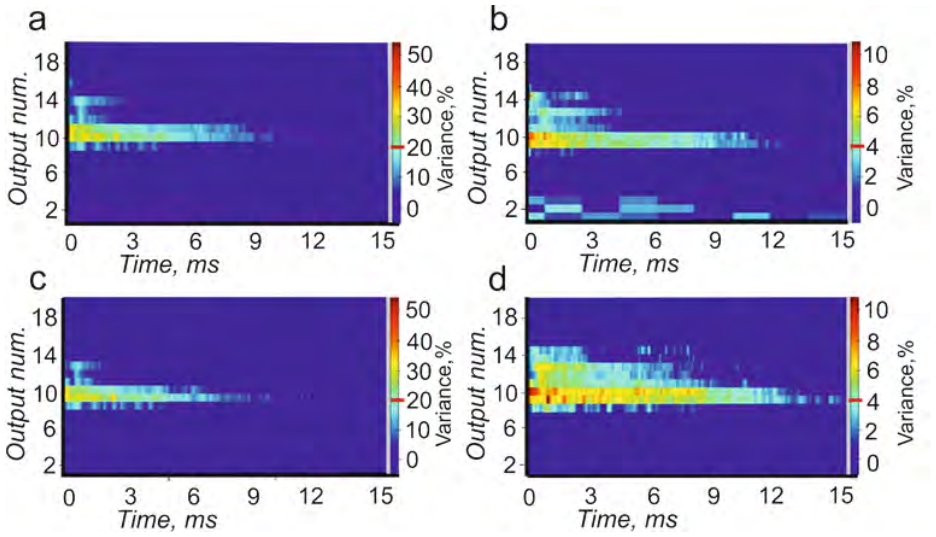

Width of frequency bands						
Output numb.	1 – 3	4 – 6	7 – 9	10 – 12	13 – 15	16 – 19
Freq. bands width, kHz	2500	625	156.25	39.062	9.765	2.4

FIGURE 6. Relative variance in the time-frequency domain for frequency bands extracted with the 4-band DWT for the categories and the subcategories in Table 1. (a) the categories discharge in TAS, discharge fail and surface discharge; the categories and the subcategories (b) discharge in TAS; pre-weakening and break-down; (c) discharge fail; no discharge and discharge tree, and (d) surface discharge; without and with pre-weakening. The horizontal marker on the scale bar defines the threshold for the features selection. The correspondence between output number and the frequency bands is given in the table below the graphs.

energies of those frequency bands were computed according to Eq. (4) and were further fed into the classifier.

D. FEATURE SPACE REDUCTION

In this work, three types of classifier were applied (i.e. SVM, FFNN and RDT) to provide a two-level classification according to the structure presented in Table 1. Hence, the first classifier differentiates the three categories and the next three classifiers separate the different subcategories. For this reason, four training datasets were formed and PCA was executed for each dataset separately. The solution of the features space reduction in the PCA is achieved by searching the elements that provide the maximum cumulative variance as described in Section III.B.

Figure 6 presents the relative variance of each individual frequency band in the time-frequency domain for the different categories and subcategories. The color encodes the relative variance, which was computed as the variance normalized by the cumulative variance. The horizontal marker on the right scale bar defines the threshold of the features that are employed for further analysis after PCA reduction. This threshold was selected after an exhaustive search to determine the optimal compromise between the classification accuracy and the features dimension. The reduction via PCA was

made to decrease the computational time without losses in accuracy.

The table in Fig. 6 gives the correspondence between the frequency bands and the output number. As can be seen, most of the variance is provided by the frequency bands ranging from 9.765 to 156.25 kHz (See Output number 7–15 in Fig. 6). In the time domain, the informative frequency bands are mostly concentrated in the time span of 0–3 ms after the discharge took place. In contrast, the features from the ***surface discharge*** subcategories (Fig. 6(d)) possess the maximum variance in the time span of 0–9 ms. Consequently, the variance for ***surface discharge*** is distributed among a greater number of features than for the other cases.

E. CLASSIFICATION TESTS RESULTS

The training of the classifiers and the tests were carried out using the datasets based on Table 1. The results of the classification tests for each category and subcategory are given in Table 3. In this table, the classification using SVM is given outside brackets as the best of the three classifier methods tested. The FFNN and RDT classifiers were less efficient as evident from the results within brackets in Table 3. The test sets for the categories incorporated also the signals from all subcategories.

In Table 3, the rows of the table contain the classification accuracy, whereas the columns represent the ground truth references. The accuracy (correct classification) was computed as the ratio of the true positives over the total number of test signals and those are highlighted in dark grey. The errors are computed as the ratio of false negatives over the total number of test signals and are in light grey. For example and for the SVM, the AE test data from the category ***discharge in TAS*** was classified with an accuracy rate of 87%. The classification error is 3% with the category ***discharge fail*** and 10% with the category ***surface discharge***.

The accuracy for the first classification level (classification of categories) in Table 3 is high considering the complexity of the process. For the categories ***discharge in TAS***, ***discharge fail*** and ***surface discharge***, they are as high as 87, 93 and 84%, respectively. These excellent results have attracted great attention due to the potential substantial economic saving in terms of energy consumption; a patent was granted [36], which demonstrate the innovative aspect of our approach.

The largest misclassification (10%) of the category ***discharge in TAS*** is made with the category ***surface discharge***. The reason is that in the category ***surface discharge***, cracks and/ or pre-weakening can take place in brittle inclusions so that the AE signals have the same duration and intensity from both events. In other words, this means that the AE of both events are expected to be similar and thus lead to some overlap of the features of both categories. In the opposite, few errors (3%) are coming from the category ***discharge fail***. This can be explained by the shorter duration and the lower intensity levels of the generated AE as compared to other signals (Fig. 4(c) and 4(d)). The second level classification for the subcategories *pre-weakening* and *break-down* has an accuracy of 85 and 89%, respectively. For the subcategory *pre-weakening*, 9% of the misclassification is made with both subcategories of ***surface discharge***. This is explained by the fact that all TAS in these subcategories have some kinds of defects either on the surface or even cracks as already shown in Fig. 4(e) and 4(f). These defects are similar to the ones occurring during ***discharge in TAS*** – *pre-weakening*.

TABLE 3. Classification test accuracy results.

Ground truth reference / *Test results accuracy in %*	***1.***	*1.1*	*1.2*	***2.***	*2.1*	*2.2*	***3.***	*3.1*	*3.2*
1. Discharge in TAS	***87 (84/86)***			*3 (4/2)*			*10 (12/12)*		
1.1 Pre-weakening		***85 (79/83)***	*4 (3/5)*			*2 (3/3)*		*5 (8/4)*	*4 (6/5)*
1.2 Break-down		*9 (11/10)*	***89 (83/89)***			*1 (1/0)*			*1 (5/1)*
2. Discharge fail	*7 (11/9)*			***93 (89/91)***					
2.1 No discharge			*3 (4/2)*		***91 (85/91)***	*6 (11/7)*			
2.2 Discharge tree		*4 (0/3)*			*3 (11/8)*	***93 (89/89)***			
3. Surface discharge	*15 (27/15)*			*1 (11/5)*			***84 (62/80)***		
3.1 Without pre- weak.		*3 (8/0)*	*5 (9/9)*					***81 (65/79)***	*11 (18/12)*
3.2 With pre- weak.			*7 (6/7)*		*1 (5/0)*			*19 (20/20)*	***73 (69/73)***

Dark grey highlight the classification match with the ground truth and light grey are the classification mistakes. The results are given as SVM (FFNN / RDT).

Therefore, it becomes obvious that the initiation of such defects produce similar AE pattern which makes their classification challenging. In contrast, the main sources of misclassification of the subcategory *Break-down* are in their mutual overlapping. This is certainly due to the proximity in terms of crack propagation of the two subcategories.

The only difference is that, in the subcategory *break-down*, the cracks propagate until the surface of the sample thus breaking the latter in several pieces. At this stage, it is important to keep in mind that the category ***discharge in TAS*** includes the *pre-weakening* and *break-down* events. Both are of upmost importance for practical applications since it has the potential to reduce significantly the costs and energy consumption of raw materials processing in mining and recycling industries.

The category ***discharge fail*** embraces the subcategories *discharge tree* and *no discharge*. This category and subcategories have the highest accuracy. This is attributed to the short duration of the signals as compared to the other categories. ***Discharge fail*** has only 7% of errors, which are in incorrect assigning with the category ***discharge in TAS***. This misclassification is certainly, for some samples, where the partial discharge was close to reaching the counter-electrode. For these samples, the duration and intensity of the AE signals is much closer to the one observed for ***discharge in TAS***. From an industrial point of view, it is very important to have a high confidence in the classification of this category as it is the one that requires additional electric discharges to achieve the desired process effect. Moreover, a too high number of ***discharge fail*** is a sign that the process is not running efficiently and the discharge parameters have to be adapted.

The category ***surface discharge*** incorporates the subcategories *with pre-weakening* and *without pre-weakening*. With a classification accuracy of 84%, this category is the least accurate. It is seen that 15% of the error is made with ***discharge in TAS*** and the mains reasons were already given. Although, this inaccuracy is not significant, it is the most critical error since a misclassification of this category with the ***discharge in TAS*** decreases slightly the process efficiency. Thus, additional investigations are pursued to enhance this classification precision. Similarly, for ***surface discharge***, the subcategories *with pre-weakening* and *without pre-weakening* remain the least accurate with 73 and 81%, respectively. However, most of the errors come from cross-classification between the two subcategories.

To mention also the classification efficiency, the SVM showed the best results as evident from Table 3. The reason may be in the rather limited training dataset, in which SVM data representation and processing is the most efficient. However, an increase of the training dataset may lead to changes in the accuracies proportions between the different classifiers, while the tremendous increase of training data probably would give equal results for all classification methods listed in this work. Unfortunately, in this specific application, the production of large datasets is very expensive. Taking into account this information, the results in Table 3 may be consider as a good compromise between the training data preparation costs and monitoring precision.

V. CONCLUSIONS AND FUTURE WORK

Pre-weakening of raw solid materials by electric discharge is a very promising method to significantly reduce the energy consumption in the mining and recycling industries. However, at present, the process monitoring is made *ex situ*, via a drop weight test method or JK Rotary Breakage. Both methods are very time and cost intensive. The lack of *in situ* and real-time monitoring systems prevents this technology to enter the market and our work aims to fulfill this gap with an innovative approach. We proposed to monitor the highly dynamical pre-weakening process by combining the acoustic emission and machine learning. The statistics of the discharges inside the solids was collected using transparent artificial samples (TAS) that were easier to inspect in terms of induced damage caused by the discharges. Three machine learning techniques were applied to the collected dataset and those were: support vector machine (SVM), feed forward neural networks (FFNN) and random decision trees (RDT). All the classifiers were tested to see whether they gave the possibility to classify correctly the discharge events. The input features for the classifier were obtained by decomposing the AE signals with data adaptive M-band (4-band) wavelets with 5 vanishing moments. The experimental results showed that wavelets were an adequate technique to grab the particularities of each individual discharge. The machine learning was capable to discover stable unique acoustic patterns that distinctly characterized the predefined categories. The limited training database (due to the high cost and time needed for samples preparation and testing in real plant) brought to different classification efficiency for each classifier. The structure of classification errors remained the same for all three types of classifiers used and the highest efficiency was achieved using SVM with radial basis kernel.

From an industrial perspective, the proposed strategy for *in situ* and real-time control of pre-weakening of solid materials using electric discharge is very promising. This is illustrated by the classification results in Table 3, where the first and second level of classification accuracies ranged from 84 to 93% and 73 to 93%, respectively. The experiments resulted in a patent application.

Still, for the category ***discharge in TAS***, some errors exist in the classification between the subcategories *pre-weakening* and *break-down.*The possible reasons are the overlapping of features within both subcategories that could not be separated precisely enough separated during the labeling and/or a diffused border between both events that needs to be quantified more precisely. The ***surface discharge*** subcategories showed the lowest classification precision. Fortunately, the errors are mainly due to a cross-classification between those two subcategories which has a limited impact on the practical applications. The reason is that for both subcategories, the TAS preserved their integrity and so requires additional electric

discharge(s). Actually, the TAS subjected to ***discharge fail*** and ***surface discharge*** categories indicate the need of additional electric discharges for further processing. To conclude, the results of the present study prove the applicability of our innovative approach is a promising solution combining AE and ML of the solid materials pre-weakening process and this can be straight forwardly transferred to *in situ* and real-time monitoring system. The further continuation of this work is the transfer to real rocks. Besides, some data adaptive classifiers can increase the analysis efficiency and both aspects are planned as a future investigation.

REFERENCES

[1] D. Tromans, "Mineral comminution: Energy efficiency considerations," *Minerals Eng.*, vol. 21, no. 8, pp. 613–620, Jul. 2008, doi: 10.1016/j.mineng.2007.12.003.

[2] M. Goldman, A. Goldman, and R. S. Sigmond, "The corona discharge, its properties and specific uses," *Pure Appl. Chem.*, vol. 57, no. 9, pp. 1353–1362, Jan. 1985, doi: 10.1351/pac198557091353.

[3] B. M. Kovalchuk, A. V. Kharlov, V. A. Vizir, V. V. Kumpyak, V. B. Zorin, and V. N. Kiselev, "High-voltage pulsed generator for dynamic fragmentation of rocks," *Rev. Sci. Instrum.*, vol. 81, no. 10, p. 103506, Sep. 2010, doi: 10.1063/1.3497307.

[4] S. H. Cho, J. H. Lee, H. M. Kang, and K. Xia, "Suggestion of dielectric breakdown strength as dynamic fracture property of rock materials," in *Rock Dynamics and Applications-State of the Art*, J. Zhao and J. Li, Eds. London, U.K.: Taylor & Francis, 2013, pp. 283–289, doi: 10.1201/b14916-33.

[5] H. Bluhm, *Pulsed Power Systems: Principles and Applications*. Berlin, Germany: Springer-Verlag, 2006, doi: 10.1007/3-540-34662-7.

[6] L. M. Tavares, "Energy absorbed in breakage of single particles in drop weight testing," *Minerals Eng.*, vol. 12, no. 1, pp. 43–50, 1999, doi: 10.1016/S0892-6875(98)00118-6.

[7] F. Shi, W. Zuo, and E. Manlapig, "Characterisation of pre-weakening effect on ores by high voltage electrical pulses based on single-particle tests," *Minerals Eng.*, vols. 50–51, pp. 69–76, Sep. 2013, doi: 10.1016/j.mineng.2013.06.017.

[8] N. N. Kencanawati and M. Shigeishi, "Acoustic emission sources of breakdown failure due to pulsed-electric discharge in concrete," *Construct. Building Materials*, vol. 25, no. 4, pp. 1691–1698, Apr. 2011, doi: 10.1016/j.conbuildmat.2010.10.013.

[9] selFrag. *selFrag-Lab Laboratory Fragmentator: Selective Fragmentation of Materials by Means of Electric Pulsed Power; 2006 Company Brochure*. Accessed: Jul. 7, 2018. [Online]. Available: http://www.sediment.uni-goettingen.de/seminar/selfrag/selFrag-Lab%20Brochure_E.pdf

[10] R. Müller-Siebert, S. F. Monti, H. Giese, and U. Friedli, "Method and device for fragmenting and/or weakening material by means of high voltage pulses," WO Patent 2014 029 034, Aug. 24, 2012.

[11] B. K. Chakrabarti and L. G. Benguigui, *Statistical Physics of Fracture and Breakdown in Disordered Systems* (Monographs on the Physics and Chemistry of Materials). Oxford, U.K.: Clarendon, 1997.

[12] V. V. Burkin, N. S. Kuznetsova, and V. V. Lopatin, "Wave dynamics of electric explosion in solids," *Tech. Phys.*, vol. 54, no. 5, pp. 644–650, May 2009, doi: 10.1134/S1063784209050065.

[13] A. Carpinteri, M. Corrado, and G. Lacidogna, "Heterogeneous materials in compression: correlations between absorbed, released and acoustic emission energies," *Eng. Failure Anal.*, vol. 33, pp. 236–250, Oct. 2013, doi: 10.1016/j.engfailanal.2013.05.016.

[14] J. Blom, J. Wastiels, and D. G. Aggelis, "Application of acoustic emission on the characterization of fracture in textile reinforced cement laminates," *Sci. World J.*, vol. 2014, Jan. 2014, Art. no. 178020. [Online]. Available: https://www.hindawi.com/journals/tswj/2014/178020/, doi: 10.1155/2014/178020.

[15] M. Ohtsu, *Acoustic Emission (AE) and Related Non-Destructive Evaluation (NDE) Techniques in the Fracture Mechanics of Concrete: Fundamental and Applications* (Series in Civil and Structural Engineering). Cambridge, U.K.: Woodhead Publishing, 2015. [Online]. Available: http://www.sciencedirect.com/science/book/9781782423270

[16] K. N. Van Dalen, "Multi-component acoustic characterization of porous media," Ph.D. thesis, Delft Univ. Technol., Delft, The Netherlands, 2013, doi: 10.1007/978-3-642-34845-7.

[17] I. Daubechies, *Ten Lectures on Wavelets* (CBMS-NSF Regional Conference Series in Applied Mathematics). Philadelphia, PA, USA: SIAM, 1992, doi: 10.1137/1.9781611970104.

[18] U. Grosse and M. Ohtsu, *Acoustic Emission Testing*. Heidelberg, Germany: Springer, 2008. [Online]. Available: http://www.springer.com/de/book/9783540698951

[19] M. Ohtsu, "Recommendation of RILEM TC 212-ACD: Acoustic emission and related NDE techniques for crack detection and damage evaluation in concrete: Test method for classification of active cracks in concrete structures by acoustic emission," *Mater. Struct.*, vol. 43, no. 9, pp. 1187–1189, Nov. 2010, doi: 10.1617/s11527-010-9640-6.

[20] L. Debnath and F. A. Shah, *Wavelet Transforms and Their Applications*, 2nd ed. Basel, Switzerland: Springer, 2015, doi: 10.1007/978-0-8176-8418-1.

[21] W. M. Telford, L. P. Geldart, and R. E. Sheriff, *Applied Geophysics*, 2nd ed. Cambridge, U.K.: Cambridge Univ. Press, 2012, pp. 283–292.

[22] A. Gupta, S. D. Joshi, and S. Prasad, "A new approach for estimation of statistically matched wavelet," *IEEE Trans. Signal Process.*, vol. 53, no. 5, pp. 1778–1793, May 2005, doi: 10.1109/TSP.2005.845470.

[23] S. G. Mallat and Z. Zhang, "Matching pursuits with time-frequency dictionaries," *IEEE Trans. Signal Process.*, vol. 41, no. 12, pp. 3397–3415, Dec. 1993, doi: 10.1109/78.258082.

[24] H. Krim, D. Tucker, S. Mallat, and D. Donoho, "On denoising and best signal representation," *IEEE Trans. Inf. Theory*, vol. 45, no. 7, pp. 2225–2238, Nov. 1999, doi: 10.1109/18.796365.

[25] A. H. Tewfik, D. Sinha, and P. Jorgensen, "On the optimal choice of a wavelet for signal representation," *IEEE Trans. Inf. Theory*, vol. 38, no. 2, pp. 747–765, Mar. 1992, doi: 10.1109/18.119734.

[26] R. A. Gopinath, J. E. Odergard, and C. S. Burrus, "Optimal wavelet representation of signals and the wavelet sampling theorem," *IEEE Trans. Circuits Syst. II. Analog Digit. Signal Process.*, vol. 41, no. 4, pp. 262–277, Apr. 1994, doi: 10.1109/82.285705.

[27] A. Aldroubi and M. Unser, "Families of multiresolution and wavelet spaces with optimal properties," *Numer. Funct. Anal. Optim.*, vol. 14, nos. 5–6, pp. 417–446, 1993, doi: 10.1080/01630569308816532.

[28] I. T. Jolliffe, "Principal component analysis," *Springer Series in Statistics*, 2nd ed. Springer, Oct. 2002, doi: 10.1007/b98835.

[29] C. Cortes and V. Vapnik, "Support-vector networks," *Mach. Learn.*, vol. 20, no. 3, pp. 273–297, Sep. 1995, doi: 10.1007/BF00994018.

[30] T. Hofmann, B. Schölkopf, and A. J. Smola, "Kernel methods in machine learning," *Ann. Stat.*, vol. 36, no. 3, pp. 1171–1220, 2008, doi: 10.1214/009053607000000677.

[31] C.-C. Chang and C.-J. Lin, "LIBSVM: A library for support vector machines," *ACM Trans. Intell. Syst. Technol.*, vol. 2, no. 3, Apr. 2011, Art. no. 27, doi: 10.1145/1961189.1961199.

[32] I. N. da Silva, D. H. Spatti, R. A. Flauzino, L. H. B. Liboni, and S. F. dos Reis Alves, *Artificial Neural Networks: A Practical Course*. Cham, Switzerland: Springer, 2017. [Online]. Available: https://www.springer.com/de/book/9783319431611

[33] L. Breiman, "Random forests," *Mach. Learn.*, vol. 45, no. 1, pp. 5–32, 2001.

[34] Z.-H. Zhou and J. Feng. (2017). "Deep forest: Towards an alternative to deep neural networks." [Online]. Available: https://arxiv.org/abs/1702.08835

[35] M. L. Wilkins, "Calculation of elastic-plastic flow," in *Methods of Computational Physics*, vol. 3. New York, NY, USA: Academic, Apr. 1963.

[36] S. Vaucher, G. Violakis, B. Meylan, S. Shevchik, K. Wasmer, and S. A. Mosaddeghi, "Method of treating a solid material by means of high voltage discharges," WO Patent 2017 214 738 A1, Jun. 15, 2016.

SERGEY A. SHEVCHIK received the engineering degree in control from the Moscow Engineering Physics Institute in 2003 and the Ph.D. degree in biophotonics from the General Physics Institute, Russia, in 2005, where he was a Post-Doctoral Researcher until 2009. From 2009 to 2012, he was with the Kurchatov Institute, Russia, developing image processing for human machine interfaces. From 2012 to 2014, he was with the University of Bern focusing on computer vision systems and multi-view geometry. Since 2014, he has been a Scientist with the Swiss Federal Laboratories for Materials Science and Technology (EMPA), developing signal processing and machine learning for industrial automatization. His research interests are in image/signal processing, pattern recognition, and machine learning.

BASTIAN MEYLAN received the B.S. and M.S. degrees in materials science and engineering from EPFL, Lausanne, Switzerland, in 2004, and 2006, and the Ph.D. degree in metallurgy from The University of Queensland, Brisbane, Australia, and 2010, respectively.

Since 2012, he has been a Scientist with the Laboratory for Advanced Materials Processing, Swiss Federal Laboratories for Materials Science and Technology (EMPA). His research interests include material processing, tribology, solidification, metallurgy, and *in situ* monitoring.

ABBAS MOSADDEGHI received the B.S., M.S., and Ph.D. degrees in electrical engineering from EPFL, Lausanne, Switzerland, in 2008, 2010, and 2014, respectively.

Since 2014, he has been with the Research and Development Department, Selfrag AG, Kerzers, Switzerland. He was a recipient of the 29th International Conference on Lightning Protection, Uppsala, Sweden, in 2008. He also received the ABB 2011 Award for his work on electromagnetic radiation from lightning return strokes to tall structures.

KILIAN WASMER (M'15) received the B.S. degree in mechanical engineering from Applied University, Sion, Switzerland, and Applied University, Paderborn, Germany, in 1999, and the Ph.D. degree in mechanical engineering from Imperial College London, U.K., in 2003.

He joined Swiss Federal Laboratories for Materials Science and Technology (EMPA), Thun, Switzerland, in 2004, to work on control of crack propagation in semi-conductors. He leads the group of dynamical processes at the Laboratory for Advanced Materials Processing. His research interests include materials deformation and wear, crack propagation prediction, and material-tool interaction. In the last years, he has focused his work on *in situ* and real-time observation of complex processes using acoustic and optical sensors in various fields such as in tribology, fracture mechanics, and laser processing.

He is the Director Committee for additive manufacturing of Swiss Engineering. He is also a member of Swiss tribology and Swissphotonics.